

## Supplementary Materials for

### **Synaptic transmission from subplate neurons controls radial migration of neocortical neurons**

Chiaki Ohtaka-Maruyama,\* Mayumi Okamoto, Kentaro Endo, Minori Oshima,  
Noe Kaneko, Kei Yura, Haruo Okado, Takaki Miyata, Nobuaki Maeda\*

\*Corresponding author. Email: maruyama-ck@igakuken.or.jp (C.O.-M.);  
maeda-nb@igakuken.or.jp (N.M.)

Published 20 April 2018, *Science* **360**, 313 (2018)  
DOI: 10.1126/aar2866

#### This PDF file includes:

Materials and Methods  
Figs. S1 to S12  
References

#### Other Supplementary Material for this manuscript includes the following: (available at [www.sciencemag.org/cgi/content/full/360/6386/313/DC1](http://www.sciencemag.org/cgi/content/full/360/6386/313/DC1))

Movies S1 to S10

## **Materials and Methods**

### Experimental animals

All animals were treated in accordance with the Tokyo Metropolitan Institute of Medical Science Animals Care and Use Committee guidelines. Pregnant ICR mice were purchased from Japan SLC, and used for *in utero* electroporation and microarray analyses. Lpar1-EGFP mice (Tg(Lpar1-EGFP)GX193Gsat) were obtained from MMRRC. TeNT-floxed mice (R26-CAG-LoxP-EGFP-TeNT) were obtained from RIKEN Bioresource Center. NR1-floxed mice were kind gifts from Dr. Takuji Iwasato.

### Antibodies

The primary antibodies used for immunostaining were rabbit anti-MAP2 (AB5622; Merck Millipore), chicken anti-GFP (ab13970, abcam), rabbit anti-VGLUT2 (#135-402; Synaptic Systems), rabbit anti-mKO (PM051M, MBL), mouse anti-PSD95 (ab13552, abcam), donkey anti-Nurr1 (AF2156, R&D systems), and rabbit anti-RFP (PM005, MBL). The secondary antibodies used were Alexa Fluor 488-conjugated donkey anti-chicken IgY (IgG) (703-545-155, Jackson ImmunoResearch), Cy5-conjugated donkey anti-rabbit IgG (711-175-152, Jackson ImmunoResearch), Alexa Fluor 546-conjugated donkey anti-rabbit IgG (A10040, ThermoFisher Scientific), and Cy5-conjugated donkey anti-mouse IgG (715-175-150, Jackson ImmunoResearch). For immunoelectron microscopy, biotin-conjugated goat anti-chicken IgY (ab97133, abcam), horseradish peroxidase (HRP)-conjugated goat anti-rabbit IgG (#458, MBL), and streptavidin-conjugated HRP (SA-5004, Vector) were used. The antibodies were used at a 1:500 dilution unless otherwise noted.

### Plasmid construction

All the cDNA fragments described below were cloned into the EcoRI sites of the pCAG-GS expression vector. pCAG-tRFP was generated by cloning the turboRFP (Evrogen) coding sequence into pCAG-GS. For construction of pCAG-GCaMP3, the GCaMP3 coding sequence was amplified by PCR using G-CaMP3 plasmid (Addgene) as a template. pCAG-SypHy was generated by cloning the synaptophysin-pHluorin coding sequence of pCMV::SypHy A4 (Addgene) into pCAG-GS. pCAG-PSD95 rescue construct was generated by insertion of a silence mutation into the sh-RNA#4 target site. The original sequence, G GTG ACG CAG ATG GAA GTG (Val-Thr-Gln-Met-Glu-Val) was changed to A GTA ACA CAA ATG GAG GTA, which didn't affect the amino acid sequence. pCAG-KikGR was generated by cloning the Kikume Green-Red coding sequence (MBL) into pCAG-GS. pCAGGS-EGFP was a gift from Dr. Ayano Kawaguchi. pCAG-Floxp-mKO2-F was a gift from Dr. Atsunori Shitamukai. pCAG-Kir2.1 was a gift from Dr. Nobuhiko Yamamoto. pCAG-Cre was a gift from Dr. Izumu Saito. p $\beta$ A-LPL-mStrawberry was a gift from Dr. Fumikazu Sudo. pEF-Cre and pT $\alpha$ -LPL-LynGFP were described previously (20).

### In utero electroporation

*In utero* electroporation was performed as previously reported (18), with some modifications. Timed pregnant mice were deeply anesthetized with sodium pentobarbital at 50 mg/kg of body weight, and the uterine horns were exposed. A plasmid DNA

solution (3-5 µg/µl) in HEPES buffered saline, pH7.2 (HBS) containing 0.01% Fast Green was injected into the lateral ventricle with a glass micropipette using a microinjector IM-31 (Narishige). Approximately 1-2 µl and 0.5 µl of plasmid solutions were injected into E14.5 and E10.5 brains, respectively. The heads of E14.5 embryos in the uterus were placed between a tweezer-type electrode 5 mm in diameter (LF650P5, BEX), and then five electric pulses (35 V, 50 ms in duration at intervals of 950 ms) were delivered using a CUY21E electroporator (BEX). For E10.5 embryos, four electric pulses (50V, 50 ms in duration at intervals of 950 ms) were applied using a 1 mm diameter disk electrode (LF650P1). After electroporation, the uterine horns were returned into the abdominal cavity to allow the embryos to continue development. In the case of *in utero* double electroporation, electroporations at E10.5 and E14.5 were successively performed using the same embryos. For the double electroporations in fig. S4, pEF-Cre (0.01 µg/µl) and pT $\alpha$ -LPL-LynGFP (0.5 µg/µl) were electroporated at E10.5, and pEF-Cre (0.00075 µg/µl) and p $\beta$ A-LPL-mStrawberry (0.3 µg/µl) were electroporated into the same embryo at E14.5 to label cells sparsely for accurately visualizing their morphology. For fig. S3, only pEF-Cre and pT $\alpha$ -LPL-LynGFP were electroporated at E10.5.

#### Immunohistochemical staining

The embryonic brains were dissected and fixed in 4% paraformaldehyde (PFA)/ PBS overnight at 4°C. The tissues were cryoprotected in 15% sucrose/ PBS for 2-3 hr, followed by 30% sucrose/ PBS overnight at 4°C. The brains were then embedded in OCT compound (Tissue Tek), and were cut into 20-µm-thick sections using a cryostat HYRAX C50 (Zeiss). The sections were soaked in PBS for 5 min, and pre-incubated with 0.01% Triton X-100/ PBS for 15 min, which were then incubated overnight at 4°C with primary antibodies diluted with PBS containing 0.5% skim milk. After washing three times with PBS, the sections were incubated with species-specific anti-IgG antibodies conjugated to Alexa Fluor 488, Alexa Fluor 546, or Cy5. Then, sections were mounted with PermaFluor (Thermo Scientific) after DAPI staining (5 µg/ml, Sigma-Aldrich). Images were captured using Zeiss LSM710, LSM780, or Leica SP8 confocal microscopes.

#### Electron microscopy

The embryonic brain samples were fixed in 2.5% glutaraldehyde (GLA)/ 0.1 M phosphate buffer, pH 7.4 (PB) at 4°C for 20 hr, and cut into coronal 200-µm-thick slices using a VT1200S microslicer (Leica). The slices were re-fixed in 2.5% GLA/ PB for 10 min, and postfixed in 1% osmium tetroxide/ PB at 4°C for 2 hr. The slices were then dehydrated in a graded series of ethanol followed by propylene oxide. Each slice was flat embedded on acclar film (Nissin EM), and polymerized in epoxy resin (EPON 812, TAAB) at 60°C for 48 hr, which was then adhered on another block of epoxy resin. Embedded slices were sectioned into 1 µm semi-thin sections using an ultramicrotome PowerTomeX (RMC Boeckeler), and stained with toluidine blue before collection for electron microscopic evaluation. 50- to 80-nm-thick ultrathin sections were cut, and placed in formvar-coated single-slot grids. After staining with uranyl acetate and lead citrate, ultrathin sections were observed under a JEM-1400 transmission electron microscope (JEOL) equipped with a bottom mount CCD camera.

### Double-label immunoelectron microscopy

pCAG-Floxp-mKO2-F (3.0 µg/µl) and pCAG-Cre (0.3 µg/µl) were electroporated into Lpar1-EGFP mouse cortices at E14.5. The electroporated brains were dissected out at E17.5, and fixed in 4% PFA/ 0.5% GLA/ 15% saturated picric acid/ 0.1 M cacodylate buffer, pH 7.3 (CB) at 4°C overnight. mKO-positive brain samples were infiltrated in 30% sucrose/ CB, and embedded in OCT compound. Then, serial 10 µm cryostat sections were cut, and used for double-label immunostaining as follows. The sections were incubated in 0.1% Triton X-100/ 50 mM Tris-buffered saline, pH 7.6 (TBST) containing 3% bovine serum albumin (BSA) at room temperature for 1 hr. Then, sections were incubated with primary antibody solution containing chicken anti-GFP and rabbit anti-mKO (1:250) in 1% BSA/ TBST at 4°C for 4 days. After 3 times washing with TBST, sections were incubated with biotin-conjugated anti-chicken IgY (1:200) in 1% BSA/ TBST at room temperature for 1 hr. After washing 3 times with TBST, sections were incubated with streptavidin-conjugated HRP (1:200) in 1% BSA/ TBST at room temperature for 1 hr. HRP signals were detected with 0.003% H<sub>2</sub>O<sub>2</sub>/ 50 mM Tris buffer, pH 7.6 (TB) containing 0.02% 3,3'-diaminobenzidine (DAB) and 1% nickel sulfate. After a 10-min coloring reaction, sections were incubated in TB overnight to stop the reaction.

After this first staining, the second staining was performed with anti-mKO antibodies. The sections were incubated in 3% BSA/ TBST for 1 hr, and then incubated with anti-mKO antibody (1:250) in 1% BSA/ TBST at 4°C overnight. After washing 3 times with TBST, sections were incubated with HRP-conjugated goat anti-rabbit IgG (1:200) for 1 hr at room temperature. After washing 3 times with TBST, the sections were incubated in 0.02% DAB/ 0.003% H<sub>2</sub>O<sub>2</sub>/ TB for 5 min. The coloring reaction was stopped in TB. The sections were mounted with AQUATEX (Merck Millipore), and observed under a Keyence BZ-X700 microscope to pick up sections containing target regions.

The sections were re-fixed with 3% GLA/ CB at 4°C for 3 days. After several rinses in 4.5% sucrose/ CB, the sections were postfixed with 2% osmium tetroxide/ 7% β-D-glucose/ 0.1 M CB for 90 min, and then with 2% osmium tetroxide/ 0.1 M CB for 1 hr at 4°C. The sections were next dehydrated in a graded series of ethanol. Subsequently, sections on glass microscope slides were horizontally infiltrated, and mounted with epoxy resin. They were polymerized at 60°C for 48 hr, and then transferred to epoxy resin blocks. From the appropriate blocks, the target regions containing contact sites between SpNs and MpNs were trimmed, and a total of 100-120 ultrathin serial sections were cut. The series of ultrathin serial sections were treated and observed as described above.

### Slice cultures

Embryonic brains electroporated with various expression constructs were dissected at E15.5 or E16.5, and embedded in 3% low-melting agarose gels prepared in HBS. Embedded brains were cut into 300-µm-thick coronal slices with a LinearSlicer PRO7 (Dosaka). The slices were placed on the insert membrane (PICMORG50, Merck Millipore), and then incubated in Neurobasal medium (Gibco) supplemented with B27 (Gibco) and antibiotics (Antibiotic-Antimycotic, Gibco) under 5% CO<sub>2</sub> and 60% O<sub>2</sub>.

### Time-lapse imaging

The slices were cultured using stage top incubators Chamlide TC (Live Cell Instrument) for SP5 and STXG-GSI2X (TOKAI HIT) for SP8 under 5% CO<sub>2</sub> and 60% O<sub>2</sub>. Time-lapse recordings, including imaging of calcium and synaptophysin-pHluorin signals, were performed using a Leica SP5 or SP8 inverted confocal microscope with a 20×long operation distance objective lens (HC PL FLUOTAR, L 20x/0.40 CORR, Leica). The maximum intensity projection was generated from 10-15 Z-stack images with 10-μm intervals at each time point. Time lapse images were collected at a single Z-plane for the GCaMP3 and synaptophysin-pHluorin imaging described in Fig. 3.

#### Calcium imaging

For calcium imaging of SpNs, pCAG-GCaMP3 was electroporated into embryonic cortices together with pCAG-tRFP at E10.5, and cortical slices were prepared at E15.5. For the Movies S9 and S10, electroporation was performed at E14.5, and the cortical slices were prepared at E16.5. The slices were cultured as described above, and two color imaging, with a 488 nm laser for GCaMP signals and a 543 nm laser for RFP signals, was performed. Relative intensity ratios of the GCaMP channel and the RFP channel were calculated and shown in a graph. Confocal images were acquired every 1 min for the Movie S5, and every 10 min for the Movie S10.

#### Synaptophysin-pHluorin imaging

pCAG-SypHy was electroporated into embryonic cortices together with pCAG-tRFP at E10.5. The electroporated brains were dissected at E16.5, and used for slice culture as described above. Two color imaging, with a 488 nm laser for synaptophysin-pHluorin signals and a 543 nm laser for RFP signals, was performed. For high K<sup>+</sup> stimulation, KCl was added into the culture medium at a final concentration of 100 mM. Confocal images were acquired every 2-3 sec.

#### Blocking of SpN activity

*In utero* double electroporation of pCAG-Kir2.1/pCAGGS-EGFP at E10.5 and pCAG-tRFP at E14.5 was performed using the same embryos as described above. The embryonic brains were dissected at E17.5, and fixed in 4% PFA/ PBS overnight at 4°C. The tissues were cut into 20-μm-thick sections, which were observed using LSM710 or LSM780 confocal microscopes as described above. Using TeNT-floxed mouse embryos, *in utero* double electroporation of pCAG-Cre/pCAGGS-EGFP at E10.5 and pCAG-tRFP at E14.5 was performed, and the brains were treated as above.

#### Glutamate uncaging

pCAG-KikGR was electroporated into cortices at E14.5, and the brain slices were prepared at E16.5. Four slices were placed on a culture dish, and MNI-caged-L-glutamate (MNI-Glu; Tocris) was added at a final concentration of 370 μM. A 405 nm laser was used to irradiate the ROI (20 μm×20 μm) below the SP for 10 sec using a Leica SP8 microscope with FRAP WIZARD software, after which the irradiated cells were converted from green to red. Multi-points time-lapse imaging of the slices in the dish containing MNI-Glu and those in the control dish without MNI-Glu was performed at the same time for 42 hr. The images were acquired every 10 min. Migrations of randomly

selected 20 neurons were analyzed for the control and treated slices from three independent experiments.

#### Primary cortical neuron culture

Primary culture of dissociated cortical neurons was performed as previously described (18). Briefly, E14.5 cortices were dissected and dissociated using papain and trituration with fire-polished Pasteur pipettes.  $1 \times 10^6$  cells were suspended in 100  $\mu$ l of medium containing 20  $\mu$ g of plasmids. Then, electroporation was performed using an electroporator CUY21 Pro-Vitro (NEPA GENE) with a cuvette electrode, where a 275 V poring pulse for 1 ms and 10 successive 20 V driving pulses for 50 ms at intervals of 50 ms were delivered. Electroporated cells were plated onto the polyethyleneimine-coated glass bottom culture dishes at a density of  $1 \times 10^5$  cells/cm<sup>2</sup>, and maintained in DMEM supplemented with 10% FBS, 0.5 mM glutamine, and Antibiotic-Antimycotic. After 3 days in culture, cells were fixed in 4% PFA/ PB at room temperature for 20 min, and subjected to immunostaining.

#### Si-RNA mediated knockdown

Short hairpin RNAs (shRNAs) were expressed in the psi-H1 vector (GeneCopoeia). Among the four clones of the OmicsLink™ shRNA Clone set for Dlg4 (PSD95) (MSH026947-CH1), clone #4(OS337692) was used for knockdown and rescue experiments. For a negative control, a shRNA scrambled control for psi-H1 (CSHCTR001-CH1) was used.

#### Conditional knock out of NMDAR

The cortices of NR1<sup>flox/flox</sup> mouse (15) embryos were electroporated with pCAG-Cre together with pCAGGS-EGFP at E14.5. Only pCAGGS-EGFP was electroporated into the littermate embryos for controls. The brains were dissected at E18.5, and fixed in 4% PFA/ PBS overnight at 4°C. Twenty- $\mu$ m-thick cryostat sections were prepared, and observed under a confocal microscope as described above.

#### Morphometric analysis

The distribution of cells and cell morphologies were analyzed after conversion of the fluorescence microscopy image into a black and white binary image using WinROOF 2015 software (Mitani Corp). The cortex was divided into the upper and lower subregions using the MAP2-immunoreactive SP as a border. In some cases, the cortex was divided into five bins. The number of the cells in each subregion (bin) was counted using a cell count program. The aspect ratios of migrating neurons were calculated using a “Particle features” algorithm.

#### FACS sorting

FACS sorting was performed using a cell sorter BD FACS Aria III (BD Bioscience). pCAGGS-EGFP was electroporated into the cortices at E14.5, and the brains were collected at E15.5, E16.5, and E17.5. GFP-positive dorsal cortical areas were dissected out under a dissection microscope with a fluorescent lamp. The tissue fragments were treated with 8-10 U/ml papain (Worthington Biochemical) and 10  $\mu$ g/ml DNase I (TAKARA Bio), and then triturated by pipetting in 10% FCS/ DMEM. Dissociated

cortical cells were collected by centrifugation (1,000×g for 5 min), and then re-suspended in HBS at a concentration of  $1\text{-}2\times10^6$  cells/ml. Dissociated cells were stained with 2 µg/ml propidium iodide (PI) prior to sorting to distinguish dead cells. The gating parameters were determined using the side and forward scatters to eliminate debris and aggregated cells, using red fluorescence (633 nm) to eliminate dead cells, and green fluorescence (488 nm) to separate the positive from negative cells. Cells prepared from the brains not electroporated with pCAGGS-EGFP were used as the negative controls. We performed FACS sorting 5-9 times to pool approximately  $2\times10^5$  GFP-positive cells for each time point, which were used for microarray analysis as described below.

#### Microarray analysis

Total RNA was purified from the collected GFP-positive cells ( $\sim2\times10^5$  cells) using Trizol (Invitrogen) according to the manufacturer's protocol. The quality of RNA was assessed with a 2100 Bioanalyzer (Agilent Technologies). Cy3-labeled cRNA was prepared using a Low Input Quick Amp Labeling Kit according to the manufacturer's protocol (Agilent Technologies). Samples were hybridized to the Mouse Gene Expression v2 Microarray (G4846A, Agilent Technologies), washed, and then scanned using a SureScan Microarray Scanner (Agilent Technologies). The microarray images were analyzed with Feature Extraction software (Agilent Technologies). Two independent microarray experiments were performed using independently prepared GFP-positive cells.

#### Data normalization and clustering analysis

The light intensity values, which correspond to the expression strength of the genes, were converted into a logarithm scale. Genes with significant difference in the expression level among E15, E16 and E17 were screened by testing whether the ranges of the expression values obtained by two measurements in each stage had no significant overlap. Assuming that the half of the range was the standard deviation (sigma), the significance level was set to 4.9 sigma, approximately p-value less than  $10^{-6}$ . After screening the genes with significant changes in the expression levels, the patterns in the changes of expression levels were clustered using the normalized expression level of E15, the normalized difference in the expression levels between E16 and E15, and the normalized difference in the expression levels between E17 and E16. By so doing, the result of the clustering would reflect differences in expression rather than the amount of expression for each day. For the distance of two genes, Euclidean distance was used and the Ward's method was used for clustering. A dendrogram was obtained by the Ward's method, which should be sliced at a certain threshold to obtain clusters. A single threshold was visually inspected so as to increase the difference in the expression pattern amongst the clusters.

#### In silico network analysis

Enrichment analysis of process networks in each cluster was performed using the web-based software MetaCore™ version 6.31 (Clarivate Analytics, Philadelphia, PA, USA).

#### Statistical analysis

Statistical analyses were performed using Graph Pad Prism 6.0 except for clustering analysis. All data were expressed as the mean  $\pm$  SEM, and Student's *t*-tests (unpaired two-tailed) were used to compare the means of two groups. Clustering analyses were performed using R statistical software (R Foundation for Statistical Computing, Vienna, Austria. URL <https://www.R-project.org/>, R core team, 2015).

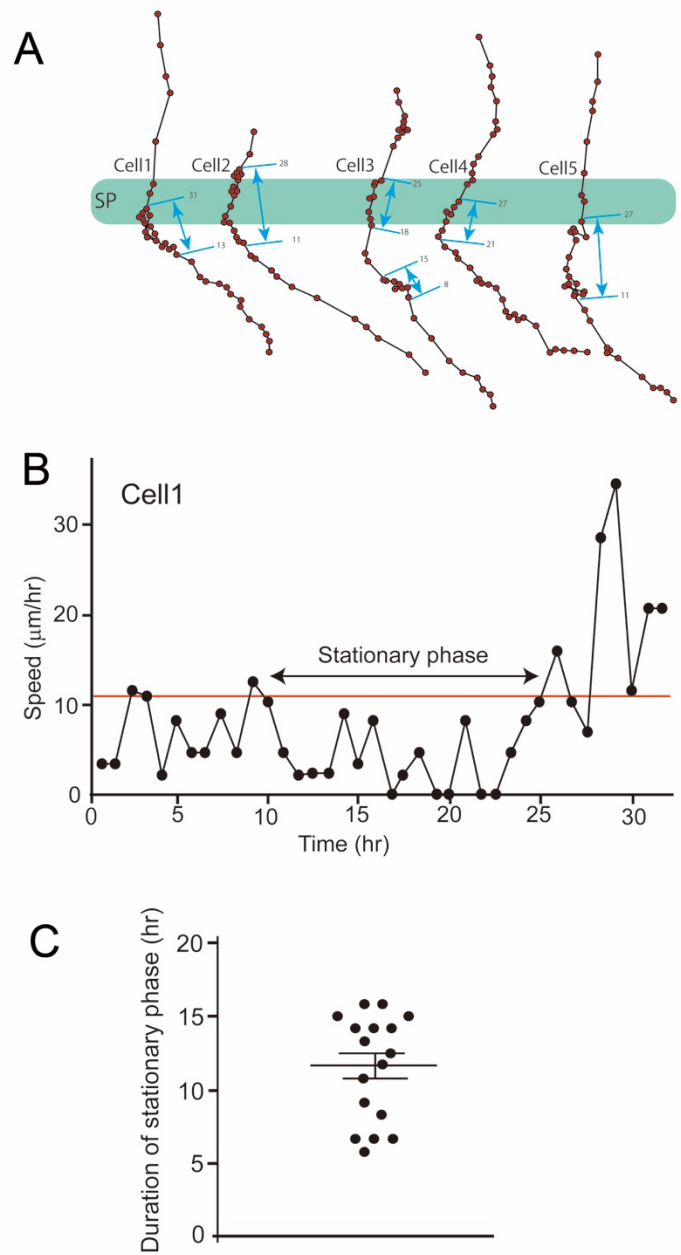


**Fig. S1. The stationary phase of MpN migration in the upper IZ and SP.** (A) The migrations of the Cells 1-5 shown in Movie S1, were tracked. The positions of the neurons were plotted every 50 min. The blue lines indicate the stationary phases of migration. Cell 3 showed stationary phases intermittently. (B) The migration speed of the Cell 1 was plotted every 50 min. The stationary phase was defined as the condition that the migration speed remained at less than 11  $\mu\text{m}/\text{hr}$  for over 5 hr. (C) The durations of the stationary phase of MpN migration around SP were plotted (N=17). We analyzed 20 neurons, and 3 of them did not show stationary phase. Error bars, mean  $\pm$  SEM.

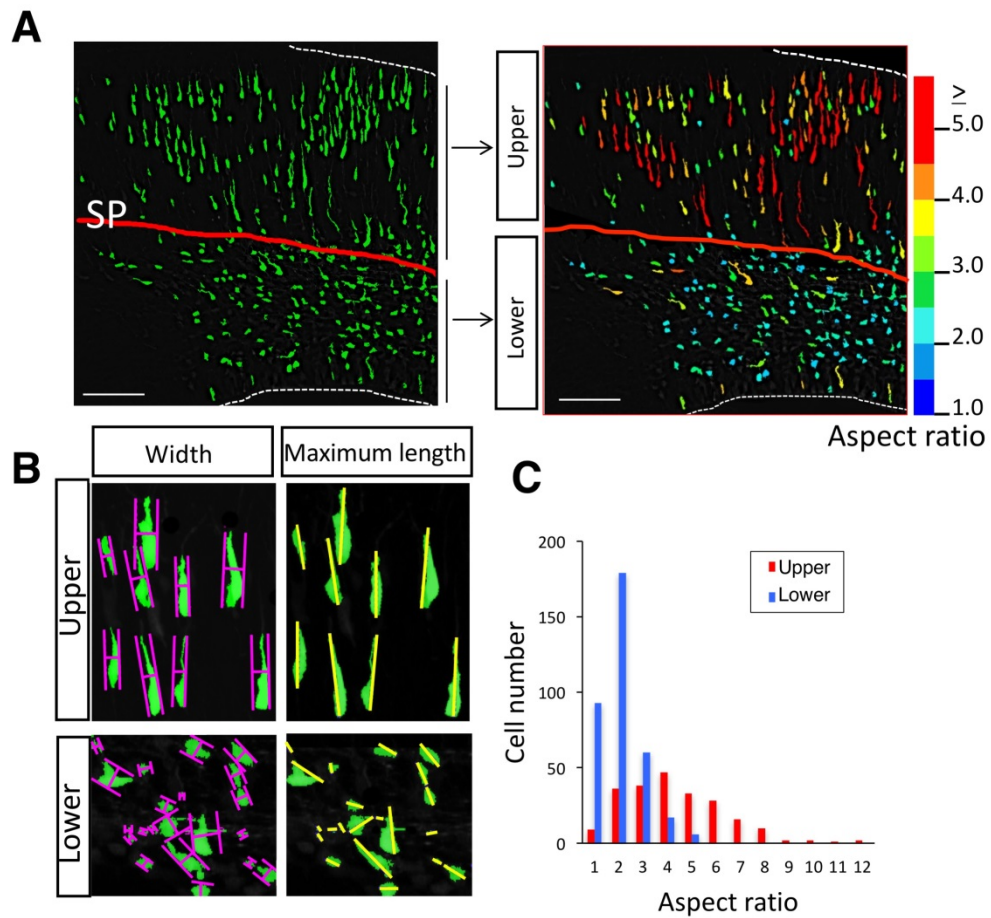


**Fig. S2. The SP is the boundary, on which the polarity of migrating excitatory neurons changes.** (A,B) Aspect ratios (maximum length/maximum width) of migrating excitatory neurons were measured using WinROOF software. The aspect ratios represented in color drastically changed at the SP. (C) While neurons with high aspect ratios were observed above the SP (red bars), most neurons below the SP exhibited low aspect ratios (blue bars). *In utero* electroporation of GFP expression plasmid was performed at E14, and the brain was fixed at E17 for morphometric analysis. Scale bars, 100  $\mu$ m.

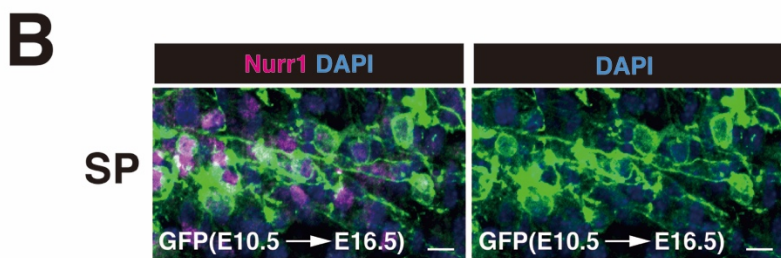
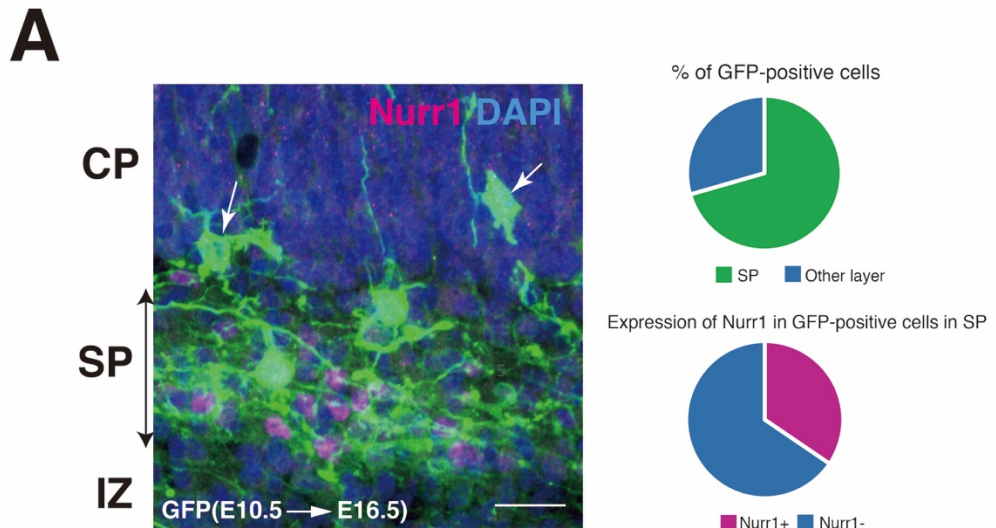


**Fig. S3. Selective labeling of SpNs by *in utero* electroporation at E10.5.** (A) *In utero* electroporation of LynGFP expression plasmids was performed at E10.5, and the brains were dissected out at E16.5. The cortical sections were immunohistochemically stained with anti-Nurr1. 70% of the GFP-positive neurons were distributed in the SP, and the rests were distributed in the deep CP (arrows). (B) 34% of the GFP-positive neurons in the SP were Nurr1-positive, which is consistent with the previous reports (6, 7). Scale bars, 20 μm for A and 10 μm for B.

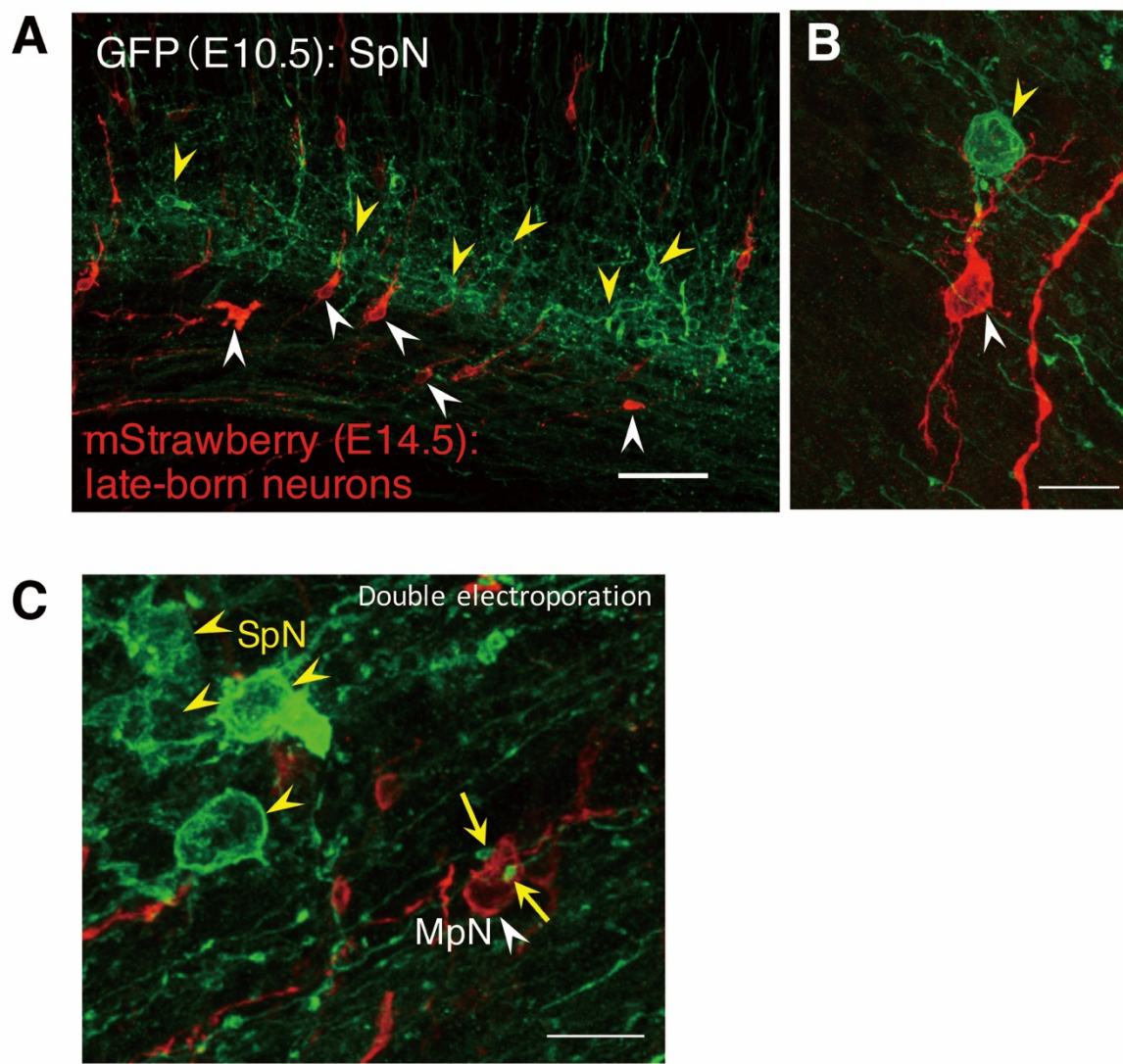


**Fig. S4. Imaging of SpNs and migrating neurons by *in utero* double electroporation.** (A to C) SpNs (yellow arrowheads) and migrating neurons (white arrowheads) were visualized by *in utero* double electroporations of LynGFP and mStrawberry expression plasmids at E10 and E14, respectively. (B) SpN and migrating neuron were closely associated with each other. (C) The contact sites often showed varicosity-like structure (arrows). Scale bars, 50  $\mu$ m for A, 10  $\mu$ m for B and C.

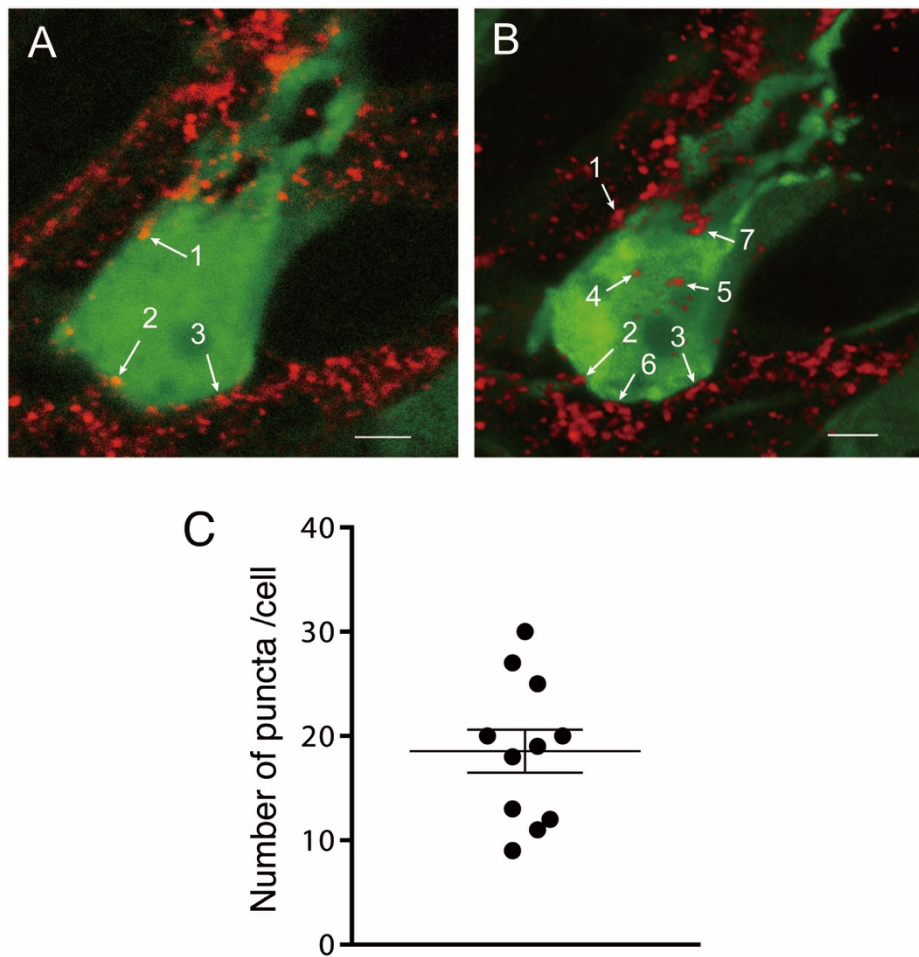


**Fig. S5. Quantification of VGLUT2-positive puncta around MpNs.** (A) E17 cortical slices that had been electroporated *in utero* with GFP constructs at E14 were immunohistochemically stained with anti-VGLUT2 antibody (red). Three VGLUT2-positive puncta were observed around an MpN (green) in a single confocal image. (B) VGLUT2-positive puncta attached to the same MpN in a reconstructed 3D image were shown. Some of the VGLUT2-positive puncta were clustered on the MpN cell body (7). (C) The numbers of VGLUT2-positive puncta around MpNs were plotted ( $N=11$ ). Only the puncta larger than 300 nm in diameter were counted. Error bars, mean  $\pm$  SEM. Scale bars, 2  $\mu$ m.

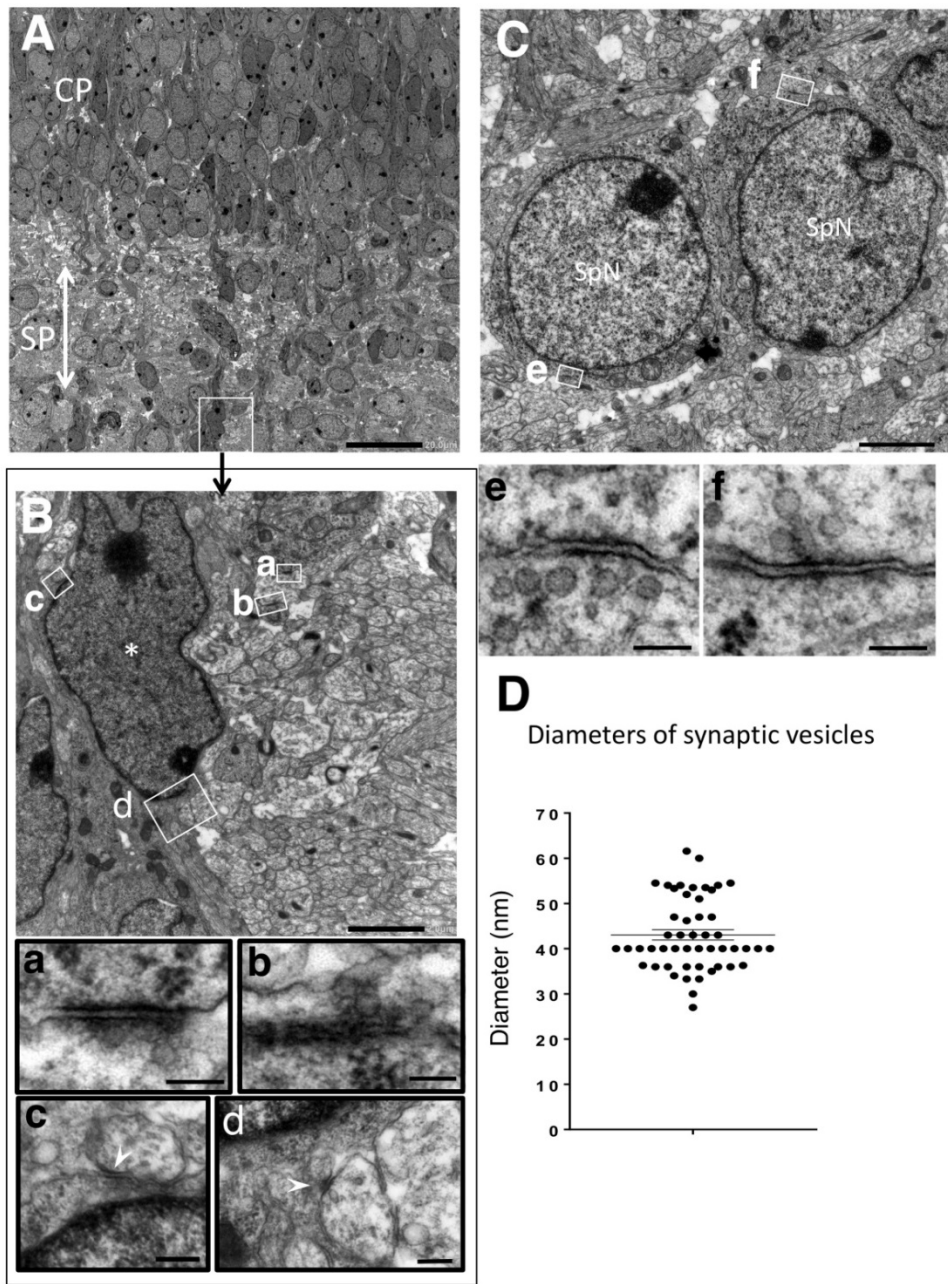


**Fig. S6. Electron microscopic analyses of the synapses on SpNs and MpNs.** (A) E16 cortical sections were observed under a transmission electron microscope. The area indicated by the rectangle is enlarged in (B). (B) The synaptic junctions formed on the MpN indicated by an asterisk were surrounded by rectangles, the areas of which are enlarged in (a)-(d). Some of them may be the immature or degenerating synaptic contacts without typical synaptic vesicles (c, d, arrowheads). (C) There were many synaptic boutons around SpN cell bodies in SP. The areas indicated by rectangles are enlarged in (e) and (f). (e, f) The synapses around SpNs were characterized by more synaptic vesicles and pale postsynaptic cytoplasm with fewer ribosomes compared with those around MpNs. (D) The diameters of the synaptic vesicles in the randomly selected 10 presynaptic regions around MpNs were plotted ( $N=50$ ). Scale bars, 20  $\mu$ m for A, 2  $\mu$ m for B and C, 100 nm for a, b, e, f, and 200 nm for c and d. Error bars, mean  $\pm$  SEM.

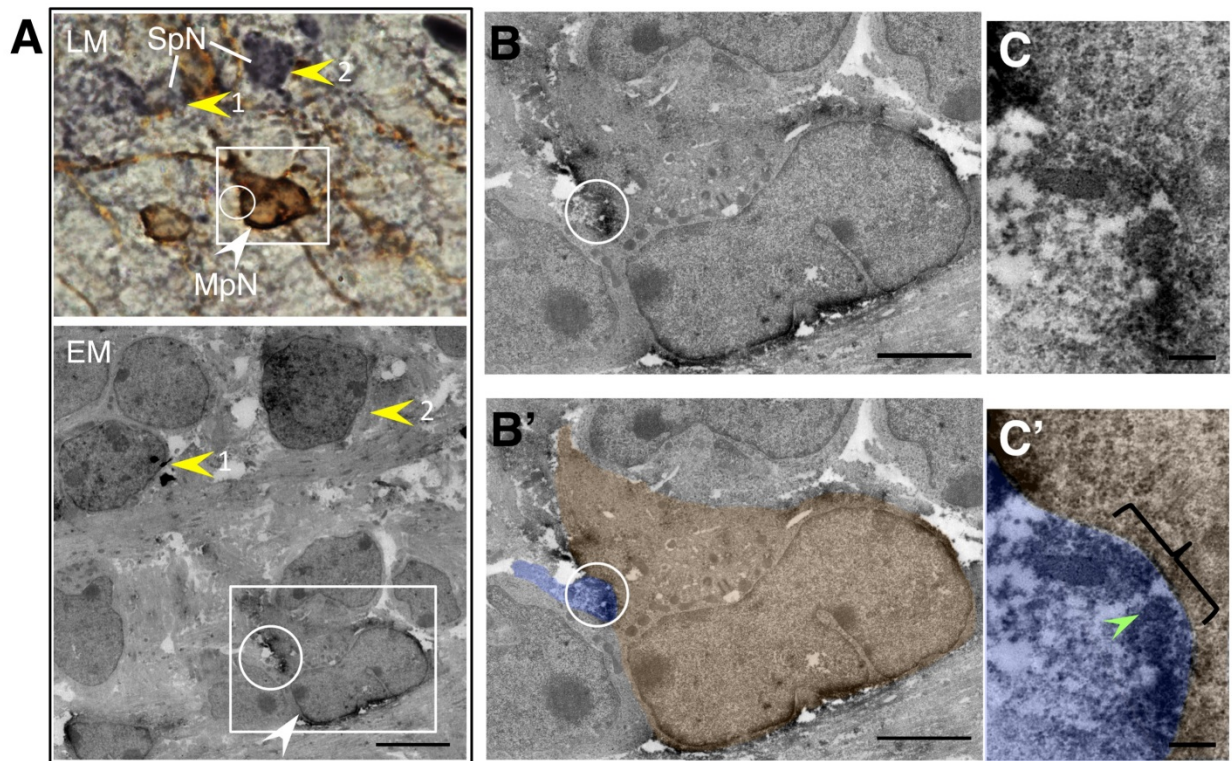


**Fig. S7. Identification of synaptic contacts between MpNs and SpNs by double-label immunoelectron microscopy.** (A) The section containing SpNs labelled with nickel-DAB (purple, yellow arrowheads) and MpNs labelled with DAB (brown, white arrowhead) were observed under an optical microscope (upper panel). Ultrathin sections were cut from this section, and the same area was observed by a transmission electron microscope (lower panel). The regions indicated by a rectangle and a circle are enlarged in (B) and (C), respectively. (B, C) A SpN process containing nickel-DAB precipitates formed synaptic contacts on the MpN cell body labeled by DAB reaction products. The SpN process is colored purple, and the MpN cell body is colored brown in (B') and (C'). The green arrowhead indicates synaptic vesicle. Scale bars, 5  $\mu$ m for A, 2.5  $\mu$ m for B, B', and 200 nm for C, C'.

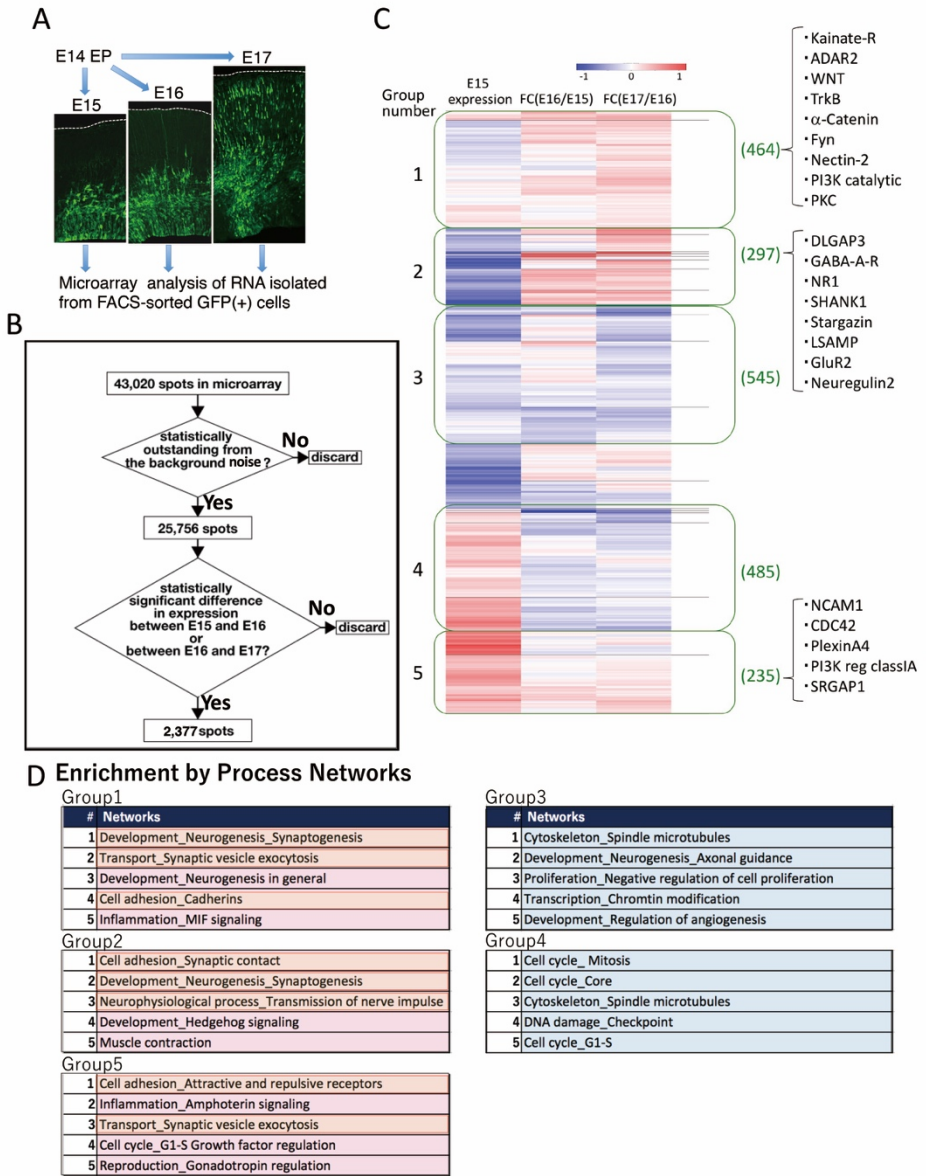


**Fig. S8. Gene expression profiling of migrating neurons.** (A) A schematic of the experiment. After *in utero* electroporation of GFP expression plasmid into E14 cortices, GFP-labelled cortical cells were collected one, two, or three days later by FACS sorting. RNAs were purified from the sorted cells and microarray analysis was performed. (B) The filtering step of data is shown in the flowchart. (C) Hierarchical clustering of the genes by their expression pattern. Expression patterns of genes in 2,377 spots were represented by two measures, namely the normalized expression level of E15, the difference in the normalized expression levels between E16 and E15, and the difference in the normalized expression levels between E17 and E16. By doing this, the result of the clustering reflected differences in expression rather than the amount of expression for each day. The number of genes in each cluster was depicted on the right side of the color-code, together with some representative protein names. (D) The top five enriched process networks analyzed by MetaCore in each group are listed.

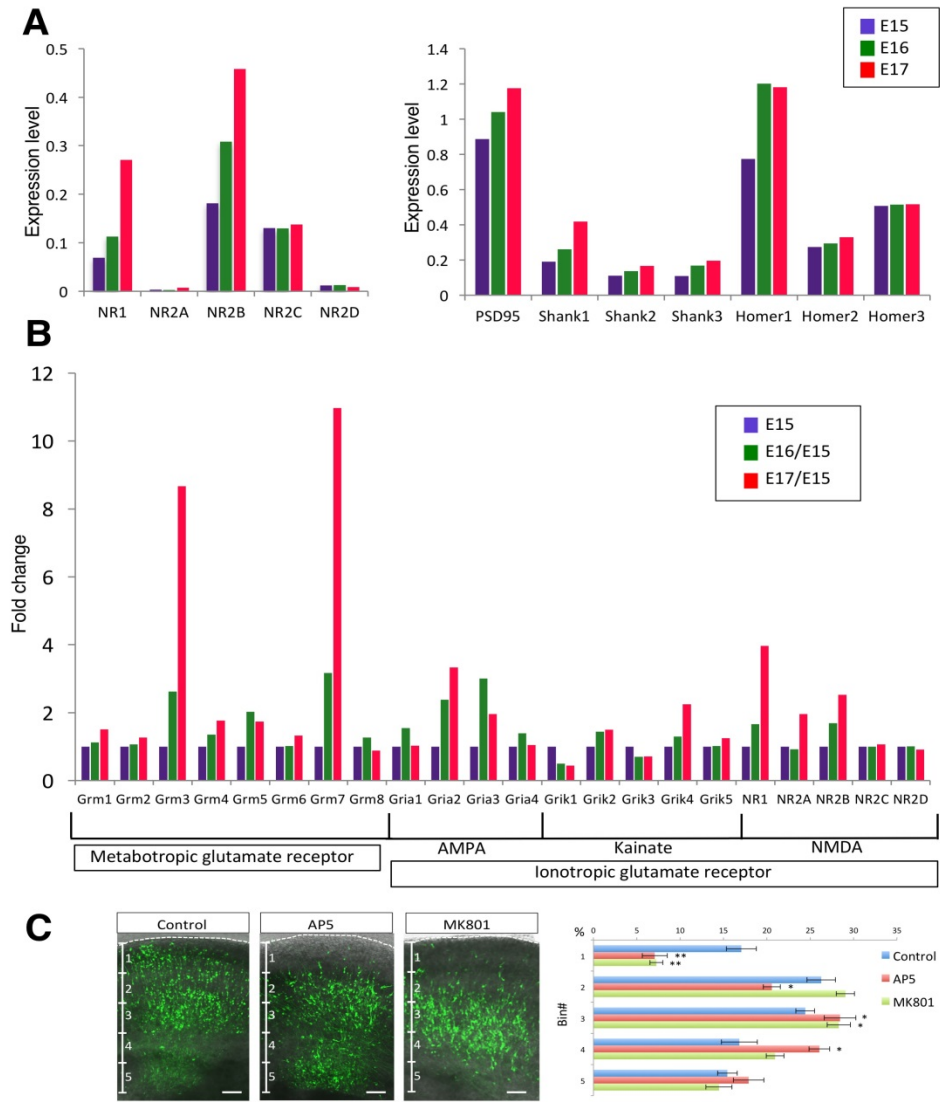


**Fig. S9. Expression of glutamate receptors during radial migration.** (A) Expression levels of NMDAR subunits and postsynaptic density proteins in migrating neurons were measured by microarray analysis described in fig. S8. Protein names are labeled at the horizontal axis. (B) Expression levels of various metabotropic and ionotropic glutamate receptors were measured as above. Gene names are labeled at the horizontal axis. MpNs showed calcium transients during multipolar-to-bipolar transition (see fig. S11), suggesting that glutamatergic synaptic transmission induces calcium signaling in MpNs. The expressions of Grm3 and Grm7 metabotropic glutamate receptors, which are linked to the inhibition of cAMP cascade, increased during migration. On the other hand, the expressions of Grm1 and Grm5, which are linked to PLC and IP<sub>3</sub>-induced Ca<sup>2+</sup> release, barely changed. Gria2 subunit, which usually prevents Ca<sup>2+</sup> influx through AMPA receptor, increased during migration. Some of the kainate receptor subunits increased during migration; however, Ca<sup>2+</sup> permeability of kainate receptors are usually low (21). We therefore focused on NMDAR. (C) Slices were prepared from E16 cortices that had been electroporated *in utero* with GFP expression plasmid at E14. Cortical slices were cultured for 3 days in the presence of AP5 or MK801 (50 μM each), and the distribution of GFP-positive neurons was evaluated. Eight (control), eleven (AP5), or seven (MK801) cortical slices were prepared using three independent pregnant mice, and subjected to morphometric analysis. Scale bars in C, 50 μm. \*P<0.05. \*\*P<0.005. Error bars, mean ± SEM.

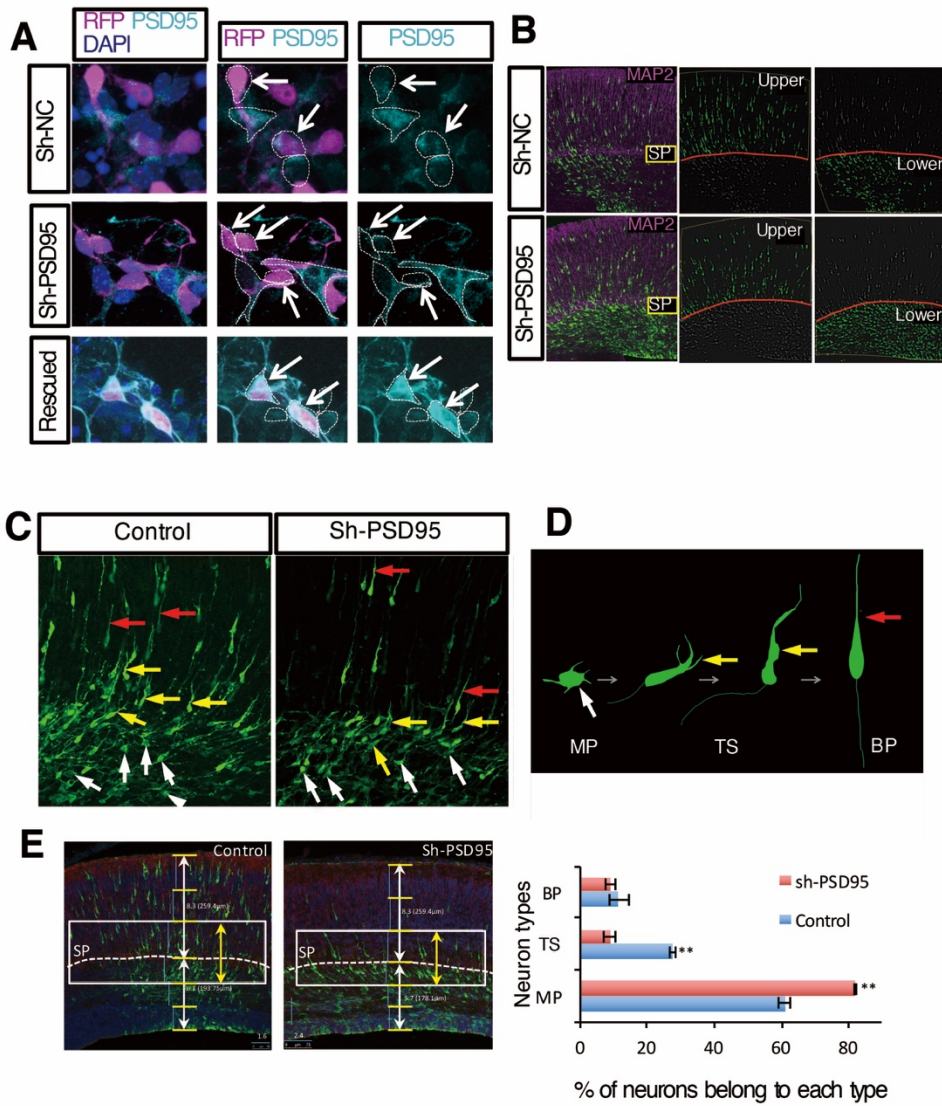


**Fig. S10. Knockdown of PSD95 impaired multipolar-to-bipolar transition.** (A) Knockdown effects on the PSD95 expression were evaluated by immunostaining with the anti-PSD95 antibody. Compared to the sh-NC construct as a control, the sh-PSD95#4 construct repressed the endogenous expression of PSD95 in primary cultured cortical neurons. PSD95 immunoreactivity was recovered by co-transfection of sh-PSD95#4 with a shRNA-resistant PSD95 expression construct. (B) Evaluation of migration defects in Fig. 4B was performed using WinROOF software. The SP layer was visualized by immunostaining with anti-MAP2, and the number of cells distributed in the regions above or below the SP was counted. (C, D) Enlarged images of Fig. 4B. In the control sections, migrating neurons exhibited three types of morphology around the SP: (1) multipolar type with multiple neurites (indicated as MP and white arrows), (2) transitional type that have a branched leading process or a swelling part at the base of the leading process (indicated as TS and yellow arrows), and (3) bipolar type with a slender unbranched leading process and a single trailing process (indicated as BP and red arrows). (E) In the knocked down sections, MP type increased and TS type decreased around the SP compared with controls. Cell types were evaluated at the areas indicated by rectangles (left). \*\*P<0.005. Error bars, mean ± SEM.

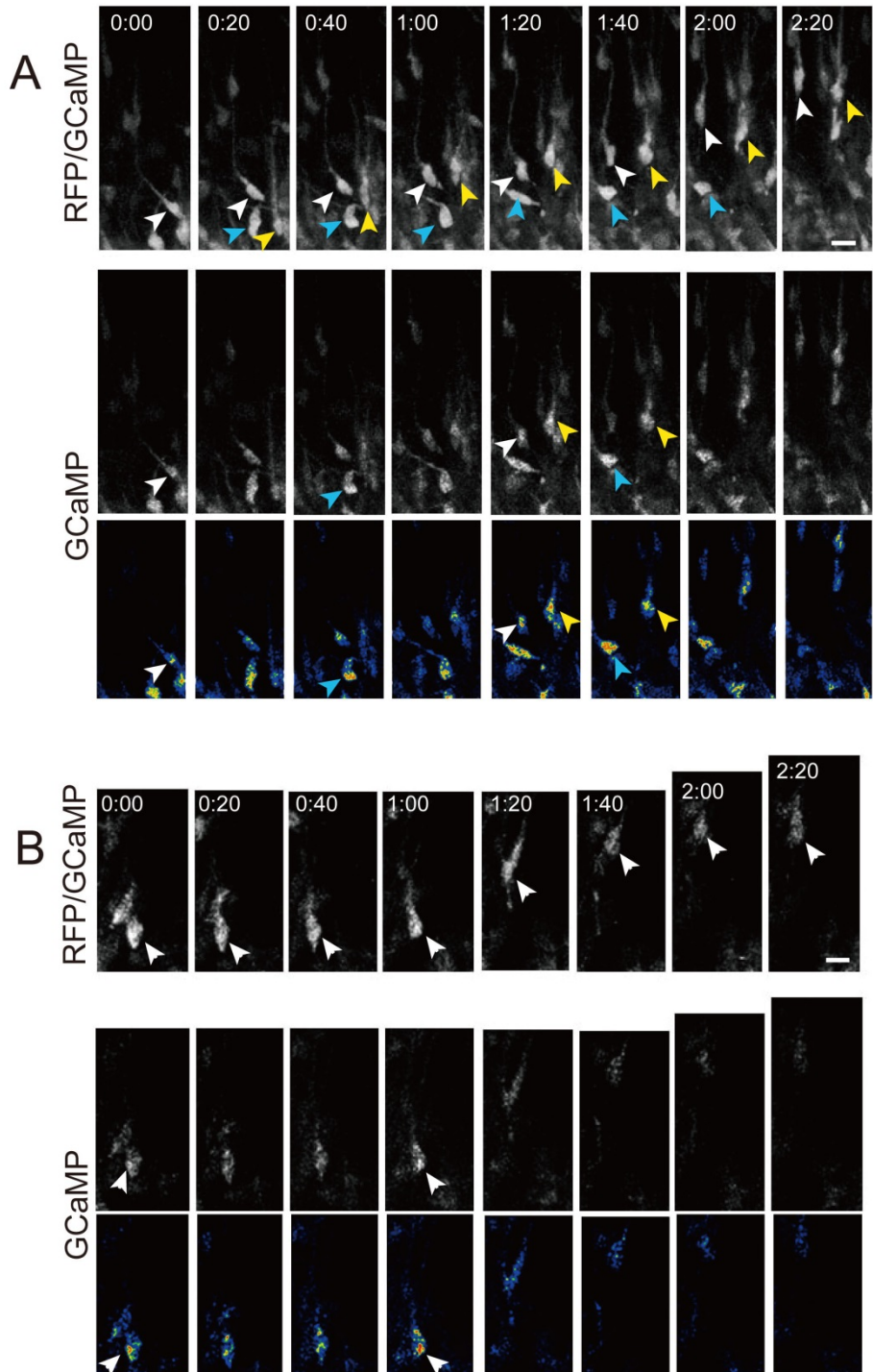


**Fig. S11. Calcium transients in MpNs during multipolar-to-bipolar transition. (A, B)**  
 Time-lapse snapshots of RFP/GCaMP3 and GCaMP3 signals in MpNs are shown. Arrowheads in the upper panels show the positions of neurons. Arrowheads in the lower panels show the  $\text{Ca}^{2+}$  rises in MpNs. We observed that about 46% of the MpNs showed  $\text{Ca}^{2+}$  transients before the initiation of locomotion. Scale bars, 10  $\mu\text{m}$ .

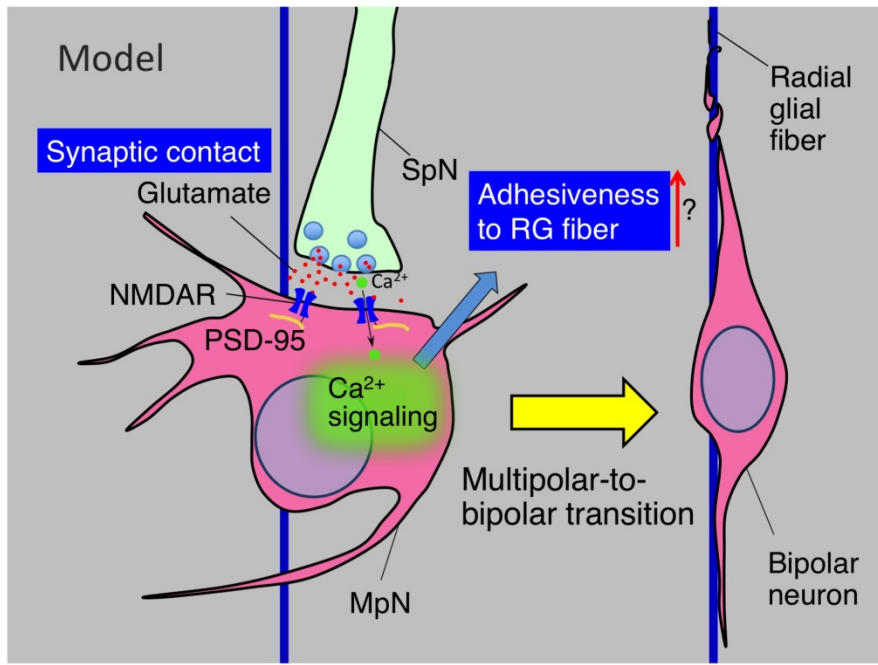


**Fig. S12. Hypothetical model for the interaction between SpNs and MpNs.** SpNs form transient glutamatergic synapses on MpNs just below the SP, which induce a Ca<sup>2+</sup> influx in MpNs through NMDARs. Calcium signaling may induce multipolar-to-bipolar transition and changes in cell adhesion.

**Movie S1. Multipolar migration switches to locomotion at the SP.** Cortical slices were prepared from E16 embryonic brains that had been electroporated with GFP expression plasmid at E14. Time-lapse imaging of the slices was performed for 45 hr. The migration paths of the Cells 1-5 are shown in Fig. S1.

**Movie S2. Extension of axon-like processes from SpNs.** Cortical slices were prepared from Lpar1-EGFP mouse brains at E16, and used for time-lapse imaging. The video shows axon-like processes vigorously extending from SpNs toward the ventricular side (arrows).

**Movie S3. 3D reconstructed image of the interaction between SpNs and MpNs.** The images of SpNs (green) and MpNs (red) in the upper IZ were reconstructed in 3D. Cortical slices were prepared from the E16 Lpar1-EGFP mouse brain that had been electroporated with RFP expression plasmid at E14.

**Movie S4. Time-lapse imaging (3D) of the interaction between SpNs and MpNs.** The Lpar1-EGFP mouse brain was electroporated with RFP expression plasmid at E14, and cortical slices were prepared at E16. Time-lapse imaging (3D) showed the presumed interaction of growing SpN neurites (arrowheads) with the cell body of MpN (red) at the upper IZ (white circle).

**Movie S5. Ca<sup>2+</sup> transients of SpNs.** SpNs showed Ca<sup>2+</sup> transients (Cells 1 and 2). In contrast, deep CP neurons barely showed Ca<sup>2+</sup> transients (Cells 3 and 4). RFP and GCaMP3 expression plasmids were introduced into SpNs by electroporation at E10. Cortical slices were prepared at E15 and used for Ca<sup>2+</sup> imaging.

**Movie S6. Imaging of pre-synaptic activity of SpNs using synaptophysin-pHluorin.** SpNs showed synaptophysin-pHluorin signals at the upper IZ. Synaptophysin-pHluorin and RFP expression plasmids were introduced into SpNs by electroporation at E10. Cortical slices were prepared at E16 and used for imaging analysis.

**Movie S7. Synaptophysin-pHluorin signals were augmented after high K<sup>+</sup> stimulation around cells below the SP.** The cortical slice used for Movie S6 was stimulated by high K<sup>+</sup> after recording under normal culture conditions. The synaptophysin-pHluorin signals were augmented after high K<sup>+</sup> stimulation around many cells in the upper IZ.

**Movie S8. Uncaging of caged glutamate stimulated locomotion by MpNs.** The slices from the E16 cortices electroporated with Kikume Green-Red construct at E14 were cultured in the presence or absence of MNI-Glu. The areas indicated by rectangles were laser-irradiated, and the migration of neurons in these areas were recorded for 40 hr.

**Movie S9 and S10. The Ca<sup>2+</sup> concentration in MpNs transiently increased at the IZ-SP boundary.** Migrating neurons were electroporated with GCaMP3 and RFP expression plasmids at E14. Cortical slices were prepared at E16, and time-lapse imaging for RFP

and GCaMP3 signals was performed. The Red channel shows the movement of an RFP-labelled MpN (arrowhead, Movie S9). This neuron exhibited a transient  $\text{Ca}^{2+}$  rise at the IZ-SP boundary just before initiation of locomotion (Movie S10).

## References

1. P. Rakic, Neurons in rhesus monkey visual cortex: Systematic relation between time of origin and eventual disposition. *Science* **183**, 425–427 (1974). [doi:10.1126/science.183.4123.425](https://doi.org/10.1126/science.183.4123.425) [Medline](#)
2. C. Ohtaka-Maruyama, H. Okado, Molecular pathways underlying projection neuron production and migration during cerebral cortical development. *Front. Neurosci.* **9**, 447 (2015). [doi:10.3389/fnins.2015.00447](https://doi.org/10.3389/fnins.2015.00447) [Medline](#)
3. J. G. Gleeson, C. A. Walsh, Neuronal migration disorders: From genetic diseases to developmental mechanisms. *Trends Neurosci.* **23**, 352–359 (2000). [doi:10.1016/S0166-2236\(00\)01607-6](https://doi.org/10.1016/S0166-2236(00)01607-6) [Medline](#)
4. K. L. Allendoerfer, C. J. Shatz, The subplate, a transient neocortical structure: Its role in the development of connections between thalamus and cortex. *Annu. Rev. Neurosci.* **17**, 185–218 (1994). [doi:10.1146/annurev.ne.17.030194.001153](https://doi.org/10.1146/annurev.ne.17.030194.001153) [Medline](#)
5. K. Sekine, K. Kubo, K. Nakajima, How does Reelin control neuronal migration and layer formation in the developing mammalian neocortex? *Neurosci. Res.* **86**, 50–58 (2014). [doi:10.1016/j.neures.2014.06.004](https://doi.org/10.1016/j.neures.2014.06.004) [Medline](#)
6. A. Hoerder-Suabedissen, F. M. Oeschger, M. L. Krishnan, T. G. Belgard, W. Z. Wang, S. Lee, C. Webber, E. Petretto, A. D. Edwards, Z. Molnár, Expression profiling of mouse subplate reveals a dynamic gene network and disease association with autism and schizophrenia. *Proc. Natl. Acad. Sci. U.S.A.* **110**, 3555–3560 (2013). [doi:10.1073/pnas.1218510110](https://doi.org/10.1073/pnas.1218510110) [Medline](#)
7. A. Hoerder-Suabedissen, Z. Molnár, Molecular diversity of early-born subplate neurons. *Cereb. Cortex* **23**, 1473–1483 (2013). [doi:10.1093/cercor/bhs137](https://doi.org/10.1093/cercor/bhs137) [Medline](#)
8. B. Granseth, B. Odermatt, S. J. Royle, L. Lagnado, Clathrin-mediated endocytosis is the dominant mechanism of vesicle retrieval at hippocampal synapses. *Neuron* **51**, 773–786 (2006). [doi:10.1016/j.neuron.2006.08.029](https://doi.org/10.1016/j.neuron.2006.08.029) [Medline](#)
9. J. Burrone, M. O’Byrne, V. N. Murthy, Multiple forms of synaptic plasticity triggered by selective suppression of activity in individual neurons. *Nature* **420**, 414–418 (2002). [doi:10.1038/nature01242](https://doi.org/10.1038/nature01242) [Medline](#)

10. M. Sakamoto, N. Ieki, G. Miyoshi, D. Mochimaru, H. Miyachi, T. Imura, M. Yamaguchi, G. Fishell, K. Mori, R. Kageyama, I. Imayoshi, Continuous postnatal neurogenesis contributes to formation of the olfactory bulb neural circuits and flexible olfactory associative learning. *J. Neurosci.* **34**, 5788–5799 (2014).  
[doi:10.1523/JNEUROSCI.0674-14.2014](https://doi.org/10.1523/JNEUROSCI.0674-14.2014) [Medline](#)
11. T. N. Behar, C. A. Scott, C. L. Greene, X. Wen, S. V. Smith, D. Maric, Q. Y. Liu, C. A. Colton, J. L. Barker, Glutamate acting at NMDA receptors stimulates embryonic cortical neuronal migration. *J. Neurosci.* **19**, 4449–4461 (1999). [Medline](#)
12. K. Hirai, H. Yoshioka, M. Kihara, K. Hasegawa, T. Sakamoto, T. Sawada, S. Fushiki, Inhibiting neuronal migration by blocking NMDA receptors in the embryonic rat cerebral cortex: A tissue culture study. *Brain Res. Dev. Brain Res.* **114**, 63–67 (1999).  
[doi:10.1016/S0165-3806\(99\)00019-X](https://doi.org/10.1016/S0165-3806(99)00019-X) [Medline](#)
13. H. Jiang, W. Jiang, J. Zou, B. Wang, M. Yu, Y. Pan, Y. Lin, Y. Mao, Y. Wang, The GluN2B subunit of N-methyl-D-aspartate receptor regulates the radial migration of cortical neurons in vivo. *Brain Res.* **1610**, 20–32 (2015). [doi:10.1016/j.brainres.2015.03.031](https://doi.org/10.1016/j.brainres.2015.03.031) [Medline](#)
14. J. J. LoTurco, M. G. Blanton, A. R. Kriegstein, Initial expression and endogenous activation of NMDA channels in early neocortical development. *J. Neurosci.* **11**, 792–799 (1991).  
[Medline](#)
15. T. Iwasato, A. Datwani, A. M. Wolf, H. Nishiyama, Y. Taguchi, S. Tonegawa, T. Knöpfel, R. S. Erzurumlu, S. Itohara, Cortex-restricted disruption of NMDAR1 impairs neuronal patterns in the barrel cortex. *Nature* **406**, 726–731 (2000). [doi:10.1038/35021059](https://doi.org/10.1038/35021059) [Medline](#)
16. B. G. Rash, J. B. Ackman, P. Rakic, Bidirectional radial  $\text{Ca}^{2+}$  activity regulates neurogenesis and migration during early cortical column formation. *Sci. Adv.* **2**, e1501733 (2016).  
[doi:10.1126/sciadv.1501733](https://doi.org/10.1126/sciadv.1501733) [Medline](#)
17. Y. Bando, K. Irie, T. Shimomura, H. Umeshima, Y. Kushida, M. Kengaku, Y. Fujiyoshi, T. Hirano, Y. Tagawa, Control of spontaneous  $\text{Ca}^{2+}$  transients is critical for neuronal maturation in the developing neocortex. *Cereb. Cortex* **26**, 106–117 (2016).  
[doi:10.1093/cercor/bhu180](https://doi.org/10.1093/cercor/bhu180) [Medline](#)

18. C. Ohtaka-Maruyama, S. Hirai, A. Miwa, J. I. Heng, H. Shitara, R. Ishii, C. Taya, H. Kawano, M. Kasai, K. Nakajima, H. Okado, RP58 regulates the multipolar-bipolar transition of newborn neurons in the developing cerebral cortex. *Cell Reports* **3**, 458–471 (2013). [doi:10.1016/j.celrep.2013.01.012](https://doi.org/10.1016/j.celrep.2013.01.012) [Medline](#)
19. G. La Fata, A. Gärtner, N. Domínguez-Iturza, T. Dresselaers, J. Dawitz, R. B. Poorthuis, M. Averna, U. Himmelreich, R. M. Meredith, T. Achsel, C. G. Dotti, C. Bagni, FMRP regulates multipolar to bipolar transition affecting neuronal migration and cortical circuitry. *Nat. Neurosci.* **17**, 1693–1700 (2014). [doi:10.1038/nn.3870](https://doi.org/10.1038/nn.3870) [Medline](#)
20. M. Okamoto, T. Namba, T. Shinoda, T. Kondo, T. Watanabe, Y. Inoue, K. Takeuchi, Y. Enomoto, K. Ota, K. Oda, Y. Wada, K. Sagou, K. Saito, A. Sakakibara, A. Kawaguchi, K. Nakajima, T. Adachi, T. Fujimori, M. Ueda, S. Hayashi, K. Kaibuchi, T. Miyata, TAG-1-assisted progenitor elongation streamlines nuclear migration to optimize subapical crowding. *Nat. Neurosci.* **16**, 1556–1566 (2013). [doi:10.1038/nn.3525](https://doi.org/10.1038/nn.3525) [Medline](#)
21. T. Yuan, C. Bellone, Glutamatergic receptors at developing synapses: The role of GluN3A-containing NMDA receptors and GluA2-lacking AMPA receptors. *Eur. J. Pharmacol.* **719**, 107–111 (2013). [doi:10.1016/j.ejphar.2013.04.056](https://doi.org/10.1016/j.ejphar.2013.04.056) [Medline](#)